Supplementary Information for:

Visualising Coordination Chemistry: Fluorescence X-ray Absorption Near Edge Structure Tomography

Simon A. James[1‡], Richard Burke[2], Daryl L. Howard[1], Kathryn M. Spiers[1‡], David J. Paterson[1], Samantha Murphy[2], Georg Ramm[2], Robin Kirkham[3], Christopher G. Ryan[3], and Martin D. de Jonge[1*]

[1]Australian Synchrotron, Clayton 3168 Australia.
[2]Monash University, School of Biological Sciences, Clayton 3800 Australia.
[3]CSIRO, Clayton 3168 Australia.

[*]Corresponding author: martin.dejonge@synchrotron.org.au.

‡ SAJ and KMS are now at the Florey Institute of Neuroscience and Mental Health (30 Royal Pde, Parkville 3052, Australia) and the Deutsches Elektronen Synchrotron – DESY (FS-PE, PETRA III Notkestrasse, 85, 22607 Hamburg, Germany) respectively.

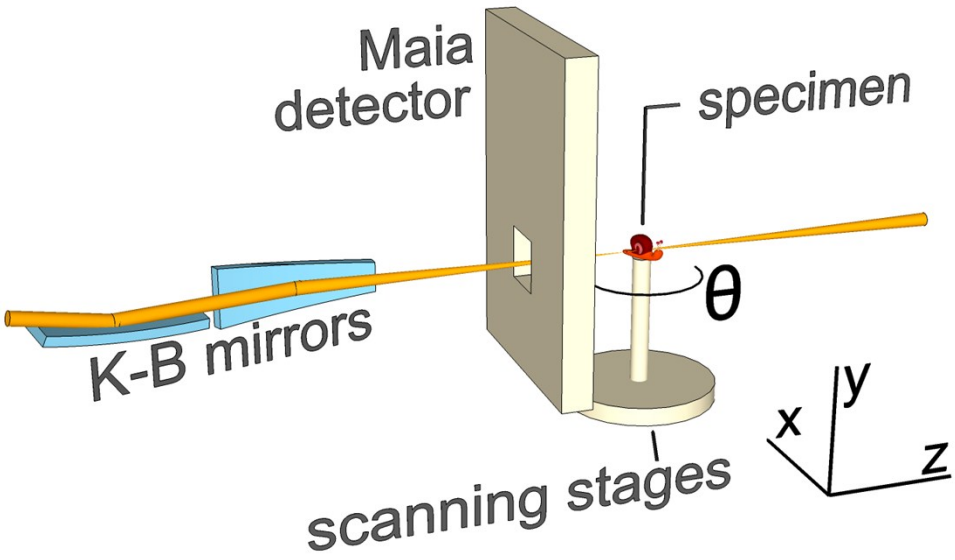

Supplementary Figure 1 | Experimental setup for XFM/φXANES. Volumetric tomography and single-slice tomographic φXANES was achieved using the Scanning X-ray Fluorescence Microprobe at the Australian Synchrotron. Monochromatic X-rays of energy, focused using a Kirkpatrick-Baez mirror pair, pass through the Maia detector before reaching a 2 μm focus in the specimen plane. Following absorption of an incident X-ray, excited atoms relax by emission of characteristic X-ray fluorescence. Images are built up by raster scanning and/or rotating about the vertical axis. Volumetric tomography was achieved by swiftly acquiring 2D projections of elemental content over a series of angular orientations (see Fig 2). Copper φXANES tomography was achieved by acquiring sinograms over a range of incident X-ray energies spanning the copper absorption edge (see Fig 2 in the main text and ESI Fig 5).

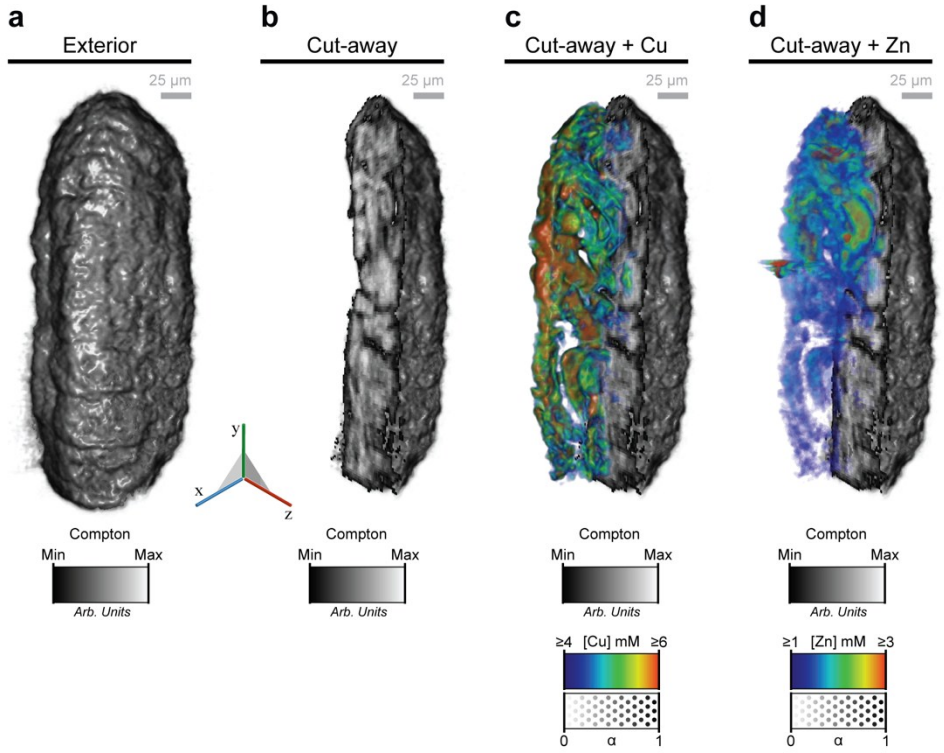

Supplementary Figure 2 | Distribution of Cu and Zn throughout *Drosophila* is tissue specific. Tomographic reconstruction of Compton scatter outlines the organic ultrastructure while reconstruction of XRF enables detailed assessment of the biometal content of intact *Drosophila* larvae (first instar). (**a**, **b**) The Compton scatter clearly defines the larval cuticle and a section reveals internal structure. Relative scattering power is shown in grey scale. Scale bar 25 µm. (**c, d**) Presenting the distribution Cu and Zn alongside the cut away from **b** reinforces the enrichment of Cu within the fat bodies. Display palette combines colour and opacity to enable visualisation of both high and low concentration distributions.

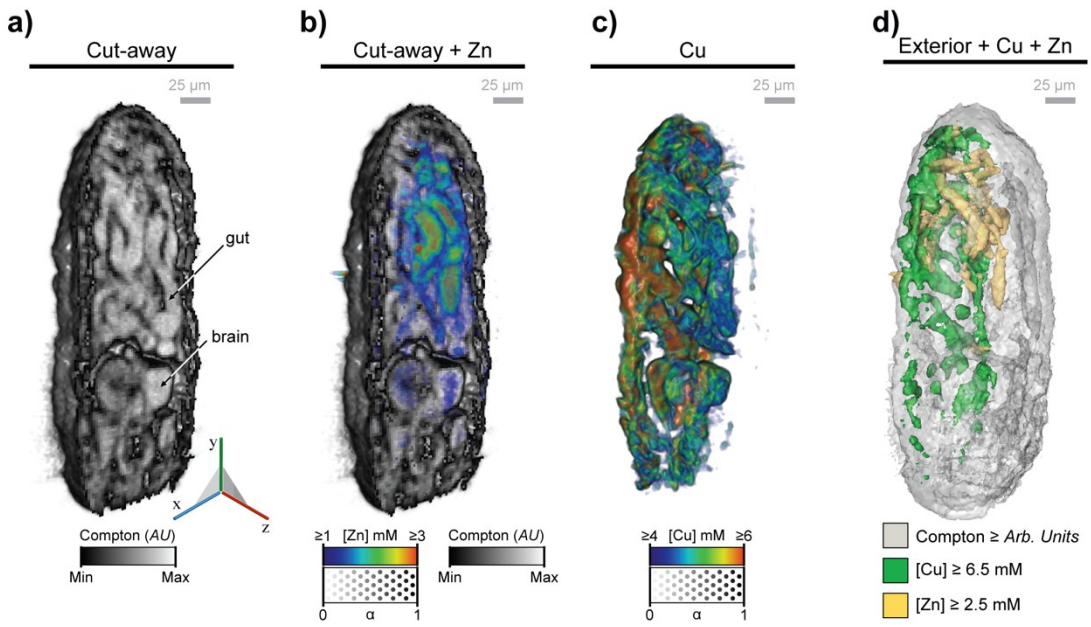

Supplementary Figure 3 | Peak concentrations of Cu and Zn are localised to specific organ structures. Two Tomographic reconstruction of inelastically (Compton) scattered photons and X-ray fluorescence (XRF) allowed visualisation of organic ultrastructure and elemental content within an intact *Drosophila* first instar larva. A virtual section (orthogonal to that shown in ESI Fig 1) through the organism allows relative differences in the intensity of Compton scatter to identify tissues such as the midgut (which contains the "copper-cells") and lobes of the developing brain. Relative scattering power displayed in grey scale. (b) Peak zinc levels are observed in the gut; Zn concentration presented using a linear colour-opacity scheme. (c) Cu is associated with all tissue structures, particularly the larval fat bodies (running along the organism's ventral surface); copper concentration is reflected using a linear colour-opacity scheme. (d) Voxels with Cu ≥ 6.5 mM and Zn ≥ 2.5 mM have been connected to form an iso-surface demarcating copper and zinc rich tissues (Grey: Compton, Cu: solid green, Zn: solid tan), allowing ready identification of the copper-rich fat bodies and zinc-rich gut. For panels (b) and (c) the range of elemental concentrations was selected to maximise the number of data points displayed while still highlighting internal structures.

Supplementary Figure 4 | Metalloarchitecture of *Drosophila* first instar larva. This movie highlights the external cuticle and the Zn distribution through the gut, but pays particular attention to visualising the high Cu concentrations in the fat bodies, the medium Cu concentrations in the gut, and the low Cu concentrations observed throughout the organism.

Supplementary Figure 5 | Cu chemistry is mapped using XANES tomography. Copper XANES tomography was achieved by recording a complete sinogram at each of 80 energies across the Cu K edge at around 8979 eV. (**a**) Depicts the energy series of sinograms – each a two-dimensional scan of position and angle – showing the Compton scatter (green) and Cu (red) maps. Measurements were recorded at 125 locations across the larva, at each of 101 orientations, and at 80 energies, and so the dataset comprises just over 1 million pixels. (**b, c**) Tomographic reconstruction illuminates the internal structure (Compton, green) throughout the energy series, and Cu XRF (red) contains information about chemical coordination. (**d**) Integrating the Cu XRF at each energy provides a single, mid-abdominal Cu XANES spectrum for bulk analysis. XANES tomography allows the complete Cu XANES spectra to be extracted from each pixel in the reconstructed image series.

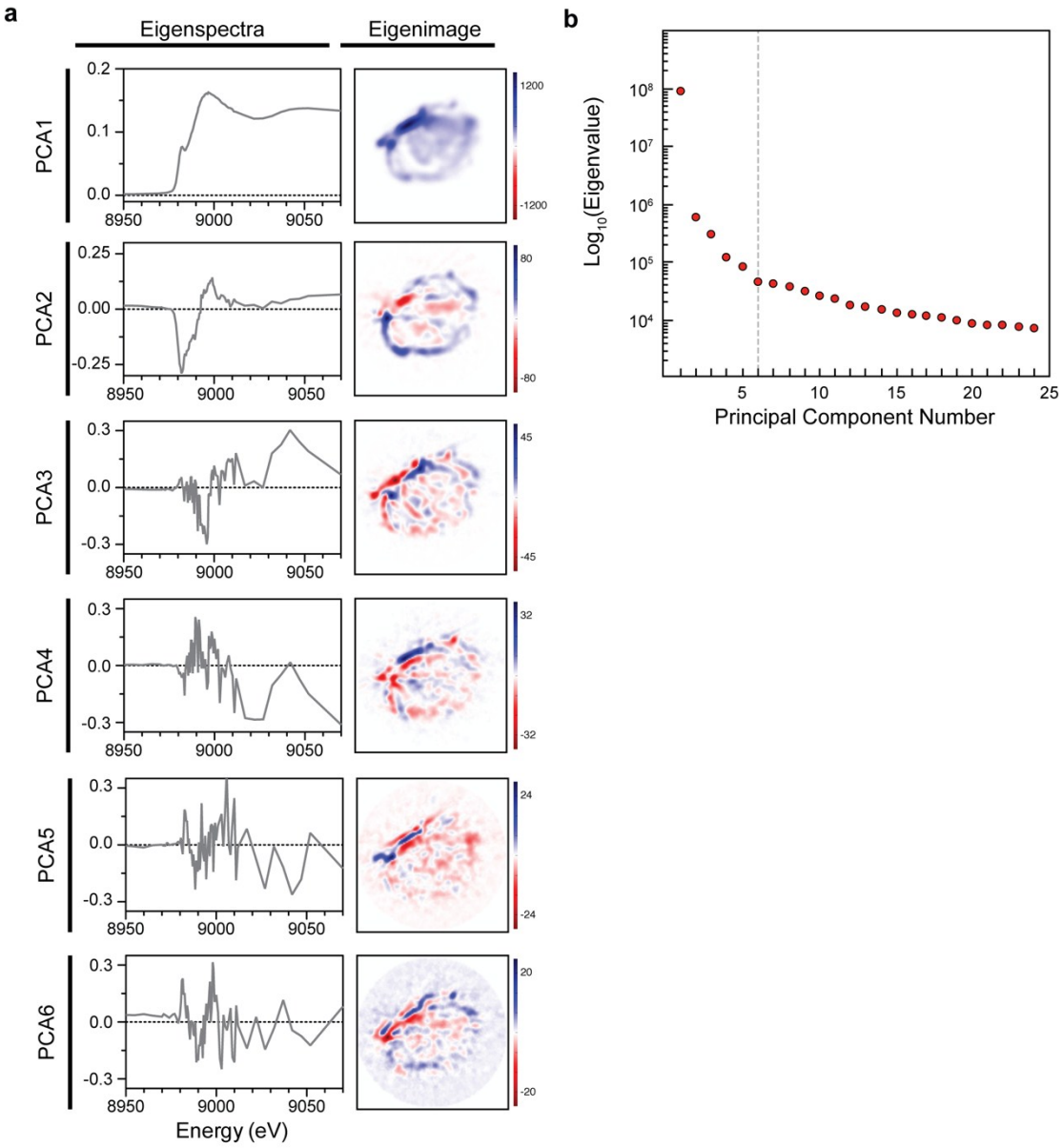

Supplementary Figure 6 | Principal component analysis (PCA) identifies the significant variations in Cu XANES spectra. PCA was used to provide a simplified description of the specimen via a series of abstract components. (**a**) The first six eigenspectra and associated eigenimages are shown and represent a reduced data matrix that retains the most meaningful information within the original data, while simultaneously separating variations in the data into successive indices of importance. PCA followed by cluster analysis (PCA-CA), as implemented by Lerotic *et al*[1], have shown this orthogonalized, noise-filtered representation of the data is a useful space within which *k*-means cluster analysis can uncover patterns in the data. (**b**) Scree plot showing $\log_{10}$(eigenvalues) as a function of principal component number.

The first 6 components account for > 99% of the observed variance and the Cattell scree test, along with inspection of the eigenspectra and eigenimages were used to exclude additional components from subsequent analyses.

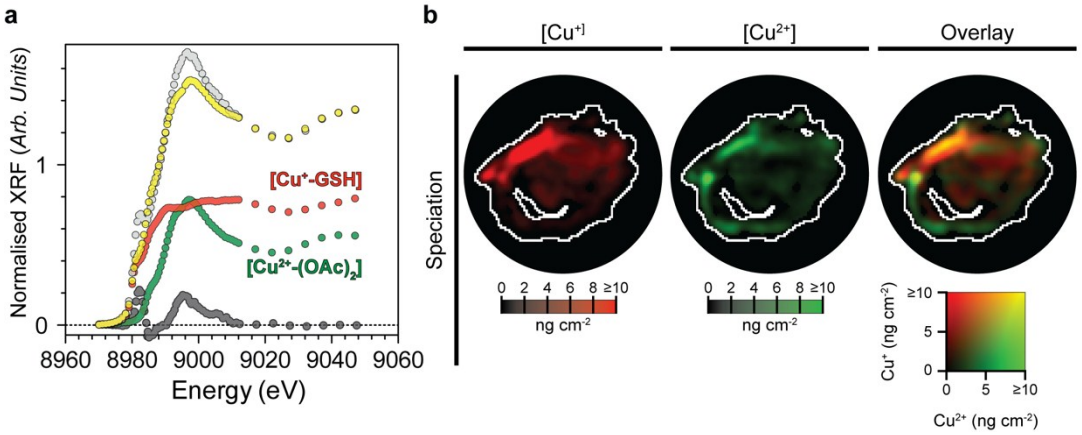

Supplementary Figure 8 | Cu^{I} and Cu^{II} rich regions are partitioned throughout *Drosophila* larvae. (**a**) Linear combination fitting (LCF) of the integrated Cu K-edge XANES spectra (8970 to 9050 eV; grey circles) identified Cu^{I}- glutathione and Cu^{II}-acetate as a two component basis set suitable for estimating the formal oxidation state of Cu at each pixel (ESI Fig S7). Areal density (ng cm^{-2}) of each Cu species is reflected using a linear colour scheme. Proportional speciation maps highlight the spatial organisation of Cu^{I} and Cu^{II} rich regions throughout the organism. Here the proportion of Cu^{I} and Cu^{II} is reflected using a linear colour scheme. These data were used to create Boolean masks capturing pixels containing 80% or more of either Cu^{I} or Cu^{II}. (**b**) The two ROIs identified in Figure 3 as predominantly Cu^{I} or Cu^{II} character, respectively. (**c**) Overlaying the Boolean mask generated in **a** with ROIs possessing the greatest Cu^{I} or Cu^{II}, seen in **b**, revealed significant spatial overlap (yellow regions). The agreement between the independent analyses presented in Figure 3 and Figure

S6 provides confidence that XANES tomography is ideally suited for mapping Cu coordination states *in situ*.

Online Methods

Reagents. Unless otherwise indicated, chemicals were purchased from Sigma-Aldrich.

***Drosophila* stocks and maintenance.** The following fly stock was used: w^{1118} (BL3605, Bloomington *Drosophila* Stock Centre, Bloomington, IN, USA) and all specimens were maintained on standard medium at 25 °C.

Sample preparation. In order to preserve structure, elemental distribution, and chemical composition as best as possible, larvae were high-pressure frozen and dried. More fully, before the larvae were loaded into the gold high pressure freezing hat (HPFH) the organisms were stored at 4 °C to slow their movement and aid selection. A wooden skewer was used to select individual larvae and load them into the HPFH before addition of 1 µl 0.7 % (w/v) low melting point agarose (to help secure the specimen) with any excess fluid wicked away. Larvae were high-pressure frozen using the Leica EMPact2 high-pressure freezer (1990 bar and -196 °C) and the larvae containing HPFH were kept submerged in liquid nitrogen until required. Successfully frozen larvae were dehydrated via freeze substitution into 2.5 % (w/v) glutaraldehyde dissolved in in acetone by placing hats into chilled fixative solution in a metal block, chilled on liquid nitrogen -196°C, and left to warm to room temp inside an insulated polystyrene container placed on a rocking platform for approx. 1.5hrs.[2] The specimens were dried by substituting the fixative step-wise for 1,1,1,3,3,3-hexamethyldisilazane (HMDS; washes: 3x Acetone, 30 % (v/v), 50 % (v/v), 70 % (v/v), 2x 100 % (v/v) HMDS, 5 min each) and allowing evaporation of the HDMS on the benchtop. The now dried larvae were mounted onto drawn glass microinjection needles ready for analysis. Samples were stored covered, in a desiccator cabinet for ~6 hrs prior to measurement.

X-ray Fluorescence Microscopy. The Kirkpatrick-Baez mirror pair installed at the XFM beamline at the Australian Synchrotron was used to focus a monochromatised beam of X-rays (see Figure 1). The incident X-ray intensity was estimated using a N_2-flowed ionisation chamber located upstream of the focussing optics. Imaging dose was estimated[3], assuming the average specimen composition to be cellulose acetate ($C_7H_8O_4$) with a density of 1.31 g cm^{-3}. While the errors of this assumed chemical composition are negligible, it is likely that the density is overestimated, resulting in a similarly overestimated dose; however, it is extremely

difficult to improve on this approach. The full-width at half-maximum of Gaussians fitted to the beam profile defined the spatial extent of illumination as ~2 μm in both the horizontal and vertical[4]. Specimens were scanned through the X-ray focus and the resulting X-ray fluorescence (XRF) and scatter were recorded using the Maia detector system[5]. Dynamic Analysis, as implemented in GeoPIXE 7.1u (CSIRO, http://www.nmp.csiro.au/GeoPIXE.html), was used to deconvolve the stream of photon events and produce elemental maps[6]. Two single-element thin metal foils of known areal density (Mn 18.9 μg cm^{-2} and Pt 42.2 μg cm^{-2}, Micromatter, Canada) were used to establish elemental quantification. As the composition and average density of the specimen were not known, nor easily estimated, cellulose acetate ($C_7H_8O_4$ and 1.31 g cm^{-3} respectively) was used to model the bulk *Drosophila*. The consequences of this choice are not significant for this study as absorption effects for Zn and Cu fluorescence are negligible for this specimen composition and size.

Volumetric Tomography of a Drosophila first instar larva. High-definition tomographic imaging (Figures 2, S1-S3) was achieved using a focussed beam of 12.85 keV X-rays. The incident X-ray intensity was 1.6×10^{10} photons s^{-1}. Acquisition was performed continuously as the specimen was raster scanned through the beam focus. Virtual pixels were defined at 2 μm intervals in each direction, and the transit time was 3.9 ms per 2 μm pixel. Four hundred projections were acquired over a full 360° of rotation. The total imaging dose delivered to the specimen was estimated at 2.2 MGy. No significant difference in elemental distribution was observed between the first (0º) and last (360º) projections and so we believe that freeze-substitution has been effective in immobilising the metals. Small features of high statistical level were used to align one series of the elemental maps, and these transferred to maps of all elements. Sinograms were reconstructed using the Gridrec algorithm implemented in IDL[7] and visualised using Amira and Chimera[8].

XANES Tomography of a Drosophila first instar larva. Copper *φ*XANES tomography was achieved by recording a sinogram of 100 orientations over 180º of rotation at each of 80 energies across the Cu K-edge at around 8979 eV (Figure S4a). Measurement energy interval was commensurate with anticipated structure in the XANES:

9152 eV to 9052 eV : 20 eV steps
9052 eV to 9012 eV : 5 eV steps
9012 eV to 9000 eV : 1 eV steps

9000 eV to 8980 eV : 0.5 eV steps

8980 eV to 8970 eV : 1 eV steps

8970 eV to 8950 eV : 5 eV steps

Transit time was 15.6 ms per 2 μm pixel, the incident X-ray intensity was around 1.1×10^{10} photons s^{-1}, and the total measurement dose estimated at 233 MGy. The entire specimen receives the same dose, and so it is telling that the chemistry has not been driven to either extreme of only one copper oxidation state dominating the speciation. Sinograms were aligned to the centre-of-mass of the Compton signal, and the Compton and Cu distributions reconstructed using the Gridrec algorithm[7] (Figure 4). The *φ*XANES tomography data set provides fewer clues as to the occurrence of radiation damage, however; the ultrastructure (as measured by the Compton scatter signal) remains intact, and the chemical speciation (as determined from the individual pixel spectra) retains strong physiological variability.

The *φ*XANES tomography imaging dose of 233 MGy is significantly lower than often imparted in a single-point measurement. This has been possible due to three main factors: (1) improved experimental efficiency enabled by the large solid angle of the Maia detector; (2) the short dwell enabled by the use of overhead-fee list-mode data acquisition, and; (3) the benefits of the dose fractionation theorem applied to tomographic analysis.[9]

***φ*XANES spectroscopy and analysis.** The *φ*XANES provides a signature of the density of states revealing electronic and structural details of the Cu coordination environment. The *φ*XANES tomography image series (see method above) was aligned by cross-correlation of the Compton reconstruction, which is essentially constant throughout the energy series. The aligned *φ*XANES image series can be thought of as a stack of images, one per energy, as displayed in Figure S4, or alternately as a collection of image pixels, each possessing a *φ*XANES spectrum. Independent analyses using Linear Combination Fitting (LCF) and Principal Component Analysis followed by Cluster Analysis (PCA-CA) assisted the exploration of the data and enabled consistency checks to determine robustness. When one has performed measurements of a complete basis set of chemical standards, LCF can be used to determine chemical composition by fitting the basis spectra to the specimen spectrum, provided that the structure in the basis chemical standards is sufficiently orthogonal and diverse. Subject to the same proviso, when the basis set is limited, one can instead use LCF to provide limited insight into gross chemical character, such as oxidation state. Here (Figure S6) we have used a limited basis set comprising copper(I) L-cysteine (Cu^{I}-Cys), copper(I) L-glutathione (Cu^{I}-

GSH), copper(II) histidine (Cu^{II}-His), copper(II) sulphate ($Cu^{II}SO_4$), Cu(I) acetate (Cu^{I}-OAc), Cu(II) acetate (Cu^{II}-$(OAc)_2$), and copper(II) ethylenediaminetetraacetate (Cu^{II}-EDTA). The basis spectra, which had been measured on a much finer energy grid, were interpolated to match the energy intervals of the specimen measurement and subsequently normalised to a unit edge jump. Initially the basis spectra were fitted to the integrated spectrum (Figure S4d), and the fit clearly preferred the basis spectra corresponding to Cu^{I}-GSH and Cu^{II}-$(OAc)_2$. While we do not propose that these are necessarily the chemical forms of Cu present in the specimen, the significant differences in the absorption edge location makes these spectra an excellent probe with which to map oxidation state in this specimen. The φXANES spectrum corresponding to each pixel was fitted to determine the component admixtures. Fit parameters were constrained to be positive. The degree of Cu^{I} / Cu^{II} character presented in Figure S7 is the result of this process. We note that the spectral data were treated anonymously, with no constraint resulting from the physical location of the pixel from which it derived, and so the spatial smoothness of the derived oxidation state maps is testament to the robustness of the measurement. PCA-CA segmentation of the φXANES stack was achieved by grouping pixels based on spectral similarity using the approach of Lerotic *et al*[1] and implemented in MANTiS v2.09 (2nd Look Consulting, http://spectromicroscopy.com).

References

1. M Lerotic, R Mak, S Wirick, F Meirer & C Jacobsen; *"MANTiS: a program for the analysis of X-ray spectromicroscopy data"*, J Synch Rad (2014), **21**: 1206 – 1212.
2. KL McDonald & RI Webb; *"Freeze substitution in 3 hours or less"*, J Micro (2011), **243**(3): 227 – 233.
3. B De Samber, S Vanblaere, R Evens, K De Schamphelaere, G Wellenreuther, F Ridoutt, G Silversmit, T Schoonjans, B Vekemans, B Masschaele, L Van Hoorebeke, K Rickers, G Falkenberg, I Szaloki, C Janssen & L Vincze; *"Dual detection X-ray fluorescence cryotomography and mapping on the model organism Daphnia magna*", Powder Diff (2010), **25**: 169 – 174.
4. J Kirz, C Jacobsen, & M Howells; *"Soft X-ray microscopes and their biological applications*", Quarterly Reviews of Biophysics (1995), **28**: 33 – 130.
5. MR Dimmock, MD de Jonge, DL Howard, SA James, R Kirkham, DM Paganin, DJ Paterson, G Ruben, CG Ryan & JMC Brown; *"Validation of a Geant4 model of the X-ray fluorescence microprobe at the Australian Synchrotron*", J Synch Rad (2015), **22**: 354 – 364.
6. CG Ryan, DP Siddons, R Kirkham, Z Y Li, MD de Jonge, DJ Paterson, A Kuczewski, DL Howard, P A Dunn, G Falkenberg, U Boesenberg, G De Geronimo, LA Fisher, A Halfpenny, MJ Lintern, E Lombi, KA Dyl, M Jensen, GF Moorhead, JS Cleverley, RM Hough, B Godel, SJ Barnes, SA James, KM Spiers, M Alfeld, G Wellenreuther, Z Vukmanovic & S Borg; *"Maia X-ray fluorescence imaging: Capturing detail in complex natural samples"*, J Phys: Conf Ser (2014), **499**: 012002.
7. CG Ryan, DP Siddons, G Moorhead & R Kirkham; *"Large detector array and real-time processing and elemental image projection of X-ray and proton microprobe fluorescence data*", Nuc Inst Meth Phys Res B (2007), **260**: 1 – 7.
8. ML Rivers, "tomoRecon: High-speed tomography reconstruction on workstations using multi-threading. in *SPIE Optical Engineering + Applications* Vol. 8506 (ed. Stock, S.R.) 85060U-85060U-13 (International Society for Optics and Photonics, 2012).

9. EF Pettersen, TD Goddard, CC Huang, GS Couch, DM Greenblatt, EC Meng & TE Ferrin; *"UCSF Chimera--a visualization system for exploratory research and analysis*", J Comput Chem (2004), **25**: 1605-1612.
10. R Hegerl & W Hoppe, *"Influence of electron noise on three-dimensional image reconstruction*", Zeitschrift für Naturforschung A (1976).